

Breaking of brightness consistency in optical flow with a lightweight CNN network

Yicheng Lin¹, Shuo Wang¹, Yunlong Jiang and Bin Han, *Member, IEEE*

Abstract—Sparse optical flow is widely used in various computer vision tasks, however assuming brightness consistency limits its performance in High Dynamic Range (HDR) environments. In this work, a lightweight network is used to extract illumination robust convolutional features and corners with strong invariance. Modifying the typical brightness consistency of the optical flow method to the convolutional feature consistency yields the light-robust hybrid optical flow method. The proposed network runs at 190 FPS on a commercial CPU because it uses only four convolutional layers to extract feature maps and score maps simultaneously. Since the shallow network is difficult to train directly, a deep network is designed to compute the reliability map that helps it. An end-to-end unsupervised training mode is used for both networks. To validate the proposed method, we compare corner repeatability and matching performance with origin optical flow under dynamic illumination. In addition, a more accurate visual inertial system is constructed by replacing the optical flow method in VINS-Mono. In a public HDR dataset, it reduces translation errors by 93%. The code is publicly available at <https://github.com/linyicheng1/LET-NET>.

I. INTRODUCTION

Optical flow estimation is a classic computer vision problem, which is widely used in object detection, feature tracking, and localization. Although optical flow has attracted the attention of many researchers, the robustness of real-time optical flow in HDR has not yet achieved the ideal performance.

Traditional variational optical flow methods, such as Lucas Kanade (LK) [1], make a series of assumptions: brightness consistency and spatial consistency. Based on above assumptions, an algebraic equation system is set up and solved by iterative optimisation methods. End-to-end optical flow methods such as FlowNet [2] use convolutional networks to extract optical flow information between image sequences directly. However, existing optical flow methods are not yet able to balance performance and efficiency in real-time applications like visual odometers. To this end, we propose a hybrid optical flow method combining convolutional network feature extraction capabilities with traditional method efficiency. It uses a lightweight network to extract illumination-invariant feature maps and score maps for follow-up pyrami-

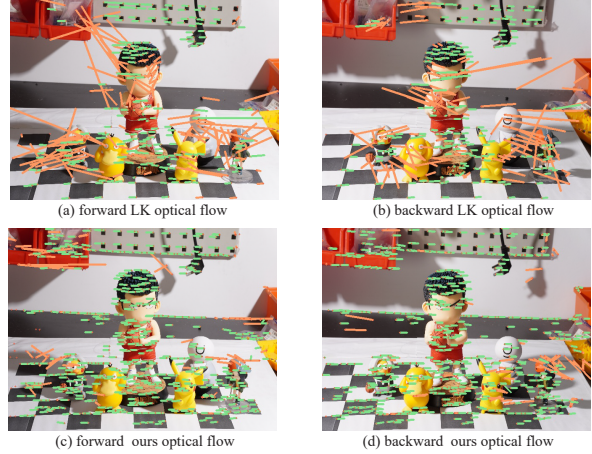


Fig. 1. Examples of dynamic lighting scene images. We collected images under different directions of light to demonstrate the robustness of the proposed method to illumination. Among them, forward optical flow refers to extracting corners in the first image and tracking them in the second image. The backward optical flow is the opposite.

dal optical flow. As shown in Fig 1, the proposed optical flow can maintain stable corner tracking under dynamic lighting conditions.

The proposed method simultaneously extracts features map F and score map S using a lightweight network. Convolution features are advanced information beyond the original RGB image with some illumination and perspective invariance. Points with higher invariance are considered corners, and these are assumed to be more stable in the optical flow. Based on the assumption that the convolution features of the same pixel in two images are invariant, we combine the traditional pyramid LK algorithm to form the robust hybrid optical flow method. In the training process, a complex network is used to extract the image reliability map R and guide the training of the lightweight network. A mask Neural Reprojection Error (mNRE) loss is used to extract local invariant features of the image, and a new peak loss is used to compute the score map.

In summary, the main contributions of this paper are as follows:

- 1) We propose a hybrid optical flow method that does not rely on brightness consistency assumptions and can work properly in HDR environments.
- 2) We propose the fastest deep learning corners and show that local information is sufficient to extract corners.
- 3) We propose a loss function mNRE for extracting local invariants in images, and improve the peaky loss in

¹These authors contributed equally to this work.

This work was supported in part by the National Natural Science Foundation of China (52375015) and in part by the Natural Science Foundation of Hubei Province of China (2022CFB239). (Corresponding author: Bin Han)

Y. Lin, S. Wang, Y. Jiang and B. Han are with the State Key Laboratory of Intelligent Manufacturing Equipment and Technology, School of Mechanical Science and Engineering, Huazhong University of Science and Technology, Wuhan 430074, China (e-mail: {yichenglin, shuowang99, jiangyunlong binhan}@hust.edu.cn).

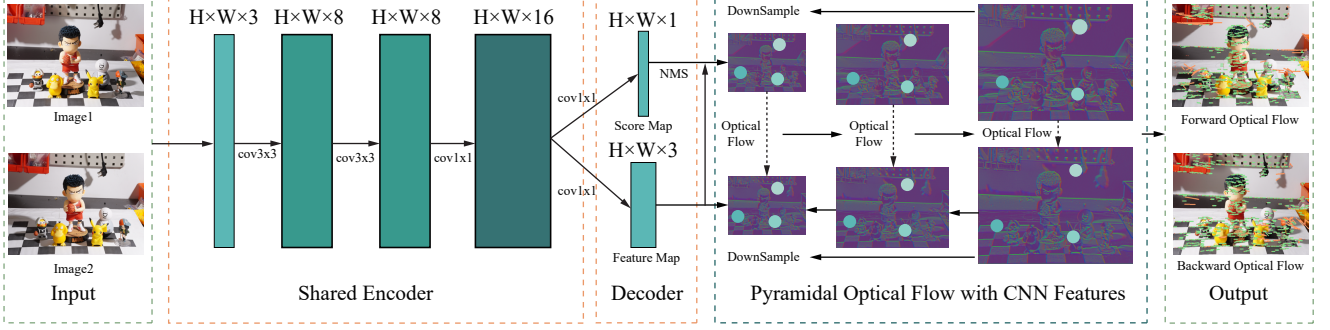


Fig. 2. **The pipeline of the proposed hybrid optical flow method.** A shared encoder is first used to extract local features of the image, and then the features are decoded into score maps S and features map F . The score map S is used to extract the tracking corners. The feature map F is used to construct the pyramidal optical flow, which is used to track the corners.

corner extraction.

- 4) We propose to use a deep network to train and a shallow network to infer, balancing performance and efficiency, reaching 190Hz on the CPU.

II. RELATED WORK

A. Traditional optical flow

Horn and Schunck (HS) [3] proposed the first truly optical flow method, which formulated optical flow estimation as an optimisation problem minimising the global energy function. Gaussian filtering has been introduced as a pre-processing operation in variational methods to improve the performance in noisy conditions [4]. To improve the robustness of illumination, [5] proposed gradient consistency and other higher-order consistency constraints, such as constancy of the Hessian and constancy of the Laplacian. In addition, [4] found that transforming RGB channels to HIS or HSV colour spaces can also improve robustness to illumination.

In contrast to HS, which computes the optical flow field for the entire image, Lucas et al [1] proposed a method to track the optical flow for specific points. To solve the problem that the displacement between pixels is not small enough in the real scene, Bouguet [6] proposed a pyramid structure to implement the coarse to fine pyramidal Lucas Kanade (PLK). Robust Local Optical Flow (RLOF) [7], [8] proposes the adjustment of the neighbourhood window size to solve the generalised aperture problem. [9] suggests that performance can be improved by selecting points that are easier to follow.

B. Learning-based optical flow

Convolutional neural networks were first used to compute optical flow by Dosovitskiy [2]. Two end-to-end networks, FlowNetS and FlowNetC, were proposed to learn optical flow directly from the synthetic annotated Flying Chairs dataset. The accuracy of the optical flow estimation in FlowNet has been improved by the addition of sub-networks for small displacements [10]. [11] introduced the pyramid model of the traditional method into the network framework, using fewer model parameters to improve the efficiency of the algorithm. Inspired by iterative updates, Recurrent All-Pairs

Field Transforms (RAFT) [12] proposed a new network architecture for optical flow estimation, and [13] further improved its detection efficiency.

C. Corner detection

Classical Harris corner detection [14] uses the autocorrelation matrix to search for corners, solving the problem of corner anisotropy and computational complexity. To enhance the tracking performance of the corners, Shi and Tomasi [15] proposed a selection criterion that makes the corners more distributed and more accurate, which has been widely used in optical flow methods. In addition, SIFT [16], ORB [17] etc. geometric invariant methods were proposed to extract corners.

Inspired by the handcrafted feature detectors, a general solution for CNN-based detection is to construct response maps to search the interest points in a supervised [18]. Super-Point [19] subsequently suggested self-supervised learning using a pre-trained model to generate pseudo-ground truth points. Furthermore, unsupervised training methods are used to extract corners, such as D2-Net [20], KeyNet [21] and others. To overcome the problem of non-differentiable Non-maximum suppression (NMS), ALIKE [22] propose differentiable feature point detection modules.

III. HYBRID OPTICAL FLOW METHOD

A. Network architecture

As illumination in Fig. 2, the network is designed to be as lightweight as possible. It completes the feature extraction function with only four convolution operations. First, image features of size $W \times H \times 16$ are extracted for the input image($W \times H \times 3$). The feature map is then transformed into a feature map and a corner score map using a 1×1 convolution network. With fewer layers and a smaller convolution kernel, the feature map contains less high-level semantic information while retaining more low-level image information. We believe that the low-level information is sufficient for our tasks. Therefore, the computational complexity of the designed network is much lower than other ones. Each of these is explained in more detail as follows:

(a) **Shared Encoder** The image feature encoder converts the input image $I \in W \times H \times 3$ to the size $W \times H \times 16$. The first two convolution operations use a 3×3 convolution kernel and expand the feature map to 8 channels. In the last layer, a 1×1 convolution kernel is used to increase the number of channels up to 16. The ReLU [23] activation function is used after each convolution. We keep the original image resolution in all convolution operations.

(b) **Feature and Score Map Decoder** The feature map is decoded into a score map and a convolution feature map by the feature decoding layer. It uses an 1×1 convolution kernel to reduce the channels of the feature map to 4. The first three channels are the convolution feature map, and the last channel is the corner score map. After the convolution, the score map is activated by the sigmoid function to limit its value between $[0, 1]$. The convolution feature map is also L2 normalised. So we get the final output with a score map of $W \times H \times 1$ and a convolution feature map of $W \times H \times 3$.

B. Optical flow with convolution feature maps

The corner is first extracted from the score map. We believe that the position with high score has strong invariance and is easy to track. After obtaining the corner position, we use it as the starting point of the optical flow. Based on the LK optical flow, we modify the brightness consistency assumption to convolution feature consistency, i.e. the convolution feature vector of the same corner position in different images is the same. Assuming that, a new hybrid optical flow method is proposed in combination with the pyramidal optical flow algorithm.

1) *Corner extraction*: The optical flow method expects a more uniform distribution of corners to improve the overall tracking robustness. So we use a method similar to the "GoodFeaturesToTrack" method in OpenCV to extract corners. First, the local maximum in the 3×3 neighbourhood is retained by NMS, and then the corners with lower scores than the threshold are removed. We then use the maximum interval sampling method to ensure a uniform distribution of the vertices.

2) *Pyramid optical flow*: In the image sequence, the convolution feature map changes with time, so it can be viewed as a function of time t and position (x, y) as $\mathbf{F}(x, y, t)$. On the assumption that the convolution feature vector of the same point remains consistent, we have:

$$\mathbf{F}(x + dx, y + dy, t + dt) = \mathbf{F}(x, y, t), \quad (1)$$

where dx and dy are the displacement of the point in the image plane, and dt is the time interval between the two images. Expanding the above equation by Taylor series, we have:

$$\begin{aligned} \mathbf{F}(x + dx, y + dy, t + dt) \\ \approx \mathbf{F}(x, y, t) + \frac{\partial \mathbf{F}}{\partial x} dx + \frac{\partial \mathbf{F}}{\partial y} dy + \frac{\partial \mathbf{F}}{\partial t} dt, \end{aligned} \quad (2)$$

where $\frac{\partial \mathbf{F}}{\partial x}$, $\frac{\partial \mathbf{F}}{\partial y}$ and $\frac{\partial \mathbf{F}}{\partial t}$ are the partial derivatives of \mathbf{F} with respect to x , y and t , respectively. Substituting the above equation into the optical flow equation:

$$\frac{\partial \mathbf{F}}{\partial x} \frac{dx}{dt} + \frac{\partial \mathbf{F}}{\partial y} \frac{dy}{dt} = -\frac{\partial \mathbf{F}}{\partial t}, \quad (3)$$

where $\frac{dx}{dt}$ and $\frac{dy}{dt}$ are the velocity of the point in the image plane. Representing the above equation in matrix form, let \mathbf{F}_x , \mathbf{F}_y and \mathbf{F}_t be the partial derivatives of \mathbf{F} with respect to x , y and t , respectively, we have:

$$[\mathbf{F}_x \quad \mathbf{F}_y] \begin{bmatrix} u \\ v \end{bmatrix} = -\mathbf{F}_t, \quad (4)$$

where u, v are the velocity of the point in the image plane and k is the number of points. Since the above equation is an overdetermined equation, the coefficient matrix is obtained by combining the optical flow equation system of multiple points:

$$\mathbf{A} = \begin{bmatrix} [\mathbf{F}_x \quad \mathbf{F}_y]_1 \\ \vdots \\ [\mathbf{F}_x \quad \mathbf{F}_y]_k \end{bmatrix}, \mathbf{b} = \begin{bmatrix} -\mathbf{F}_{t1} \\ \vdots \\ -\mathbf{F}_{tk} \end{bmatrix}. \quad (5)$$

It can then be solved by standard least squares:

$$\begin{bmatrix} u \\ v \end{bmatrix}^* = -(\mathbf{A}^T \mathbf{A})^{-1} \mathbf{A}^T \mathbf{b}. \quad (6)$$

IV. LEARNING TRACKED CORNERS AND INVARIANT FEATURE

We use the same shallow network parameters to calculate the score map S and convolution feature map F for a set of images in the dataset, as shown in Fig. 3. The dense descriptor map D is extracted by a VGG-like multi-scale deep network, supervising the reliability map R of the corners. Based on the work of ALIKE [22], we also use the reprojection loss function, repeatability loss function and peaky loss function to extract the corner score map. In addition, for the problem of fast convergence to straight edges when extracting corners, we propose a line peaky loss based on the idea of hard sample mining. The NRE [24] loss function for calculating global features is combined with a local mask to obtain a loss function that only considers local invariance.

A. Learning corners with high invariance

Three loss functions are used to train for the extraction of corners. The reprojection loss function and peaky loss function are designed to ensure the accuracy of the corners, and the dense descriptor map D will supervise the reliability of the corners. The specific loss functions are shown as follows:

1) *Reprojection loss*: A point \mathbf{p}_a in image \mathbf{I}_A is projected to image \mathbf{I}_B , and the projection point is \mathbf{p}_{AB} . The single reprojection error is:

$$\text{dist}_{AB} = \|\mathbf{p}_{AB} - \mathbf{p}_B\|_p, \quad (7)$$

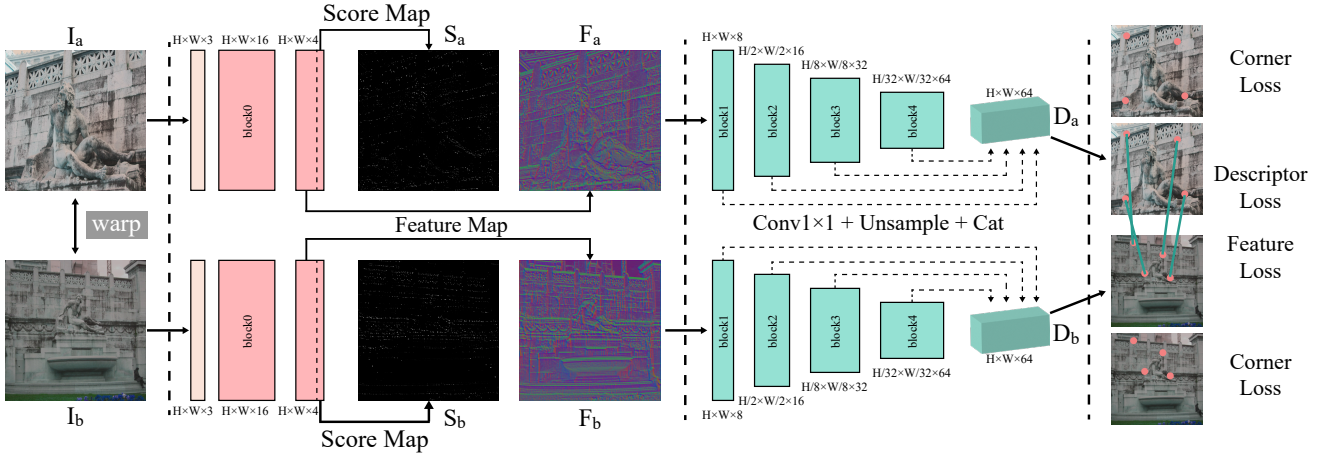


Fig. 3. **The network training process.** A shallow network is first used to extract the score map S and feature map F . Then, in order to supervise the reliability of the training corners, a deep convolution is used to extract the dense descriptor map D . Finally, we calculate the corner loss and matching loss based on the results of $[S, F, D]$.

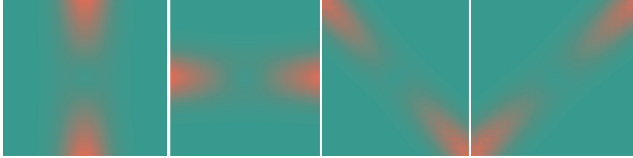


Fig. 4. **Visualisation of the weights of the four line models.** Four line models represent vertical, horizontal, left oblique, and right oblique lines, respectively. The weight values shown in the figure are the product of the distance $d(i, j)$ and the formula 9.

where \mathbf{p}_B is the ground truth point in image \mathbf{I}_B . The reprojection error loss is defined in a symmetrical form:

$$\mathcal{L}_{rp} = \frac{1}{2}(\text{dist}_{AB} + \text{dist}_{BA}). \quad (8)$$

2) *Line peaky loss:* We hope that the scores at other locations near the corner will show a peak state. In previous work [22], the score of the all surrounding points was used for the calculation, which led to a slow decrease in the score map after convergence to a straight line. Therefore, we propose four line model weights for the most difficult straight edge samples, as shown in Fig. 4. The maximum loss value under the four line models will be adopted to make the score map converge quickly to the peak state. The specific weight calculation formula is as follows:

$$\begin{aligned} w_1(i, j) &= \mathcal{N}(|i - \hat{i}|), \\ w_2(i, j) &= \mathcal{N}(|j - \hat{j}|), \\ w_3(i, j) &= \mathcal{N}(|i + j - \hat{i} - \hat{j}|), \\ w_4(i, j) &= \mathcal{N}(|i - j - \hat{i} + \hat{j}|), \quad 0 \leq i, j < N, \end{aligned} \quad (9)$$

where \mathcal{N} is the Gaussian function, (\hat{i}, \hat{j}) is the coordinate of the corner point, and N is the size of the local window. Then the maximum value under the four line models is adopted

as the loss function:

$$\mathcal{L}_{pk} = \frac{1}{N^2} \max_{i=1 \dots 4} \left\{ \sum_{0 \leq i, j < N} w_i(i, j) d(i, j) s(i, j) \right\}, \quad (10)$$

where $d(i, j)$ and $s(i, j)$ are the distance and score of the point (i, j) , respectively.

3) *Reliability loss:* As mentioned in the previous work [20], [22], the accuracy of the corner is not enough, and the reliability of the corner needs to be ensured. Therefore, we use the dense descriptor map D to supervise the reliability of the corners. As in ALIKE [22], the reliability of the corner $r_{\mathbf{p}_A}$ is calculated in the same way. Then the reliability loss function is defined as:

$$\mathcal{L}_{reliability}^A = \frac{1}{N_A} \sum_{\substack{\mathbf{p}_A \in \mathbf{I}_A \\ \mathbf{p}_{AB} \in \mathbf{I}_B}} \frac{s_{\mathbf{p}_A} s_{\mathbf{p}_{AB}}}{\sum_{\substack{\mathbf{p}'_A \in \mathbf{I}_A \\ \mathbf{p}'_{AB} \in \mathbf{I}_B}} s_{\mathbf{p}'_A} s_{\mathbf{p}'_{AB}}} (1 - r_{\mathbf{p}_A}) \quad (11)$$

where N_A is the number of corners, and $s_{\mathbf{p}_A}$ is the score of the corner \mathbf{p}_A . Similar to the reprojection function, we also define the symmetrical form of the reliability loss function:

$$\mathcal{L}_{rl} = \frac{1}{2} (\mathcal{L}_{reliability}^A + \mathcal{L}_{reliability}^B). \quad (12)$$

B. Learning invariant features map

The NRE [24] loss function is used by many works to calculate the global consistency of the descriptor. We modified it by adding a local mask to obtain a loss function that only considers local invariance. Specifically, we first define a mask near the corner \mathbf{p} :

$$\text{mask}(\mathbf{p}) = \begin{cases} 1 & \text{if } \max(|x - \mathbf{p}_x|, |y - \mathbf{p}_y|) < d \\ 0 & \text{otherwise} \end{cases} \quad (13)$$

where (x, y) is the coordinate of the pixel, and $(\mathbf{p}_x, \mathbf{p}_y)$ is the coordinate of the corner \mathbf{p} . Similar to ALIKE [22], the mNRE loss function is modified as:

$$\begin{aligned} mNRE(\mathbf{p}_A, \text{warp}_{AB}, \mathbf{d}_{\mathbf{p}_A}, \mathbf{D}_B) \\ = -\ln(\text{mask}(\mathbf{p}_A) \cdot q_m(\mathbf{p}_{AB} | \mathbf{d}_{\mathbf{p}_A}, \mathbf{D}_B)) \end{aligned} \quad (14)$$

where warp_{AB} is the warping function, $\mathbf{d}_{\mathbf{p}_A}$ is the descriptor of the corner \mathbf{p}_A , and \mathbf{D}_B is the dense descriptor map of image \mathbf{I}_B . Finally, we get a loss function that only considers local invariance:

$$\begin{aligned} \mathcal{L}_{mNRE} = & \frac{1}{N_A + N_B} \\ & \left(\sum_{\mathbf{p}_A \in \mathbf{I}_A} mNRE(\mathbf{p}_A, \text{warp}_{AB}, \mathbf{d}_{\mathbf{p}_A}, \mathbf{D}_B) + \right. \\ & \left. \sum_{\mathbf{p}_B \in \mathbf{I}_B} mNRE(\mathbf{p}_B, \text{warp}_{BA}, \mathbf{d}_{\mathbf{p}_B}, \mathbf{D}_A) \right) \end{aligned} \quad (15)$$

V. EXPERIMENTS

In this section, we first introduce the training details. To validate the proposed method, we first compare the corner repeatability on the HPatches [25] dataset. Then, several image sets captured under dynamic lighting environments are used to verify the proposed optical flow performance in HDR environments. Finally, the proposed method is embedded in a modern VIO system and the trajectory accuracy is compared to verify its effectiveness in practical use.

A. Training Details

MegaDepth [26] is used to train the model. It contains 63k images from 135 famous scenes and provides the corresponding poses, depths and densities between frames. All images in the dataset are scaled to 480×480 during the training process. Training is done using the ADAM [27] optimiser with a learning rate of $3e^{-3}$. We set the batch size to one, but use the gradient of 16 batches to accumulate, and train for 100 epochs. Using the above settings, our model was trained on a 4090 graphics card for approximately one day.

B. HPatches Repeatability

In order to verify the performance of the proposed model in the detection of corners, we calculated the repeatability of the corners on the HPatches [25] dataset. We compared the proposed method with ALIKE(T) [22], SuperPoint [19], Harris [14], Fast [28], Random. Among them, ALIKE(T) and SuperPoint are deep learning based methods for detecting features and extracting descriptors. The repeatability is calculated for the extraction of 300 corners at a resolution of 240×320 . The same non-maximum suppression is used for all feature point detection methods to suppress the phenomenon of feature point clustering. The feature points with reprojection distance less than 3 in the two images are considered to be repeat corners and the feature points above this threshold are not repeatable. The comparison of repeatability in illumination scenes and viewpoint scenes is shown in the table I. We can see that the proposed corner point repetition rate is at the state-of-the-art level.

In terms of calculation time, all methods are run on the same CPU and measured. We computed the non-deep learning corner extraction method in the size of 480×640 , and computed the deep learning corner score map in 240×320 , and then upsampled to 480×640 . From the table I, it can be

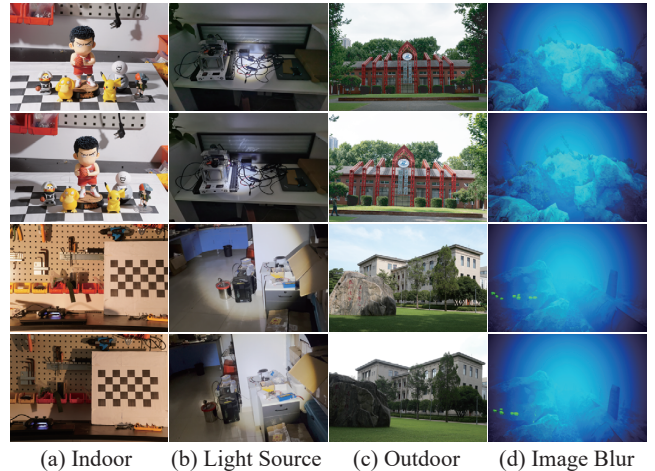


Fig. 5. **Examples of dynamic lighting scene images.** The collected data contains four typical scenes, indoor light source changes, outdoor sunlight changes, active light sources and image blur caused by light scattering. The gray scale assumption is not satisfied in all image pairs.

seen that the proposed method has greatly improved the real-time performance compared to other deep learning solutions, and even comparable to traditional methods.

TABLE I
REPEATABILITY COMPARISON

Method	Repeatability		CPU time(ms)
	Illumination Scenes	Viewpoint Scenes	
Ours	0.618	0.606	5.2
ALIKE(T) [22]	0.638	0.563	84.4
SuperPoint [19]	0.652	0.503	93.5
Harris [14]	0.62	0.556	4.9
Fast [28]	0.575	0.552	0.4
Random	0.101	0.1	/

C. Corner Tracking

To verify the performance of the proposed flow in dynamic lighting scenes, we collected several sets of image pairs with typical lighting changes and active searchlight sequences. Fig. 5 shows some examples of collected image pairs. All of them do not fulfil the assumption of grey scale invariance. We divide these scenes into four typical categories, namely indoor light source changes, outdoor sunlight changes, active light sources and image blur caused by light diffusion. Each category collects five pairs of images with small angle differences but large illumination changes.

Using the collected data, we compared the proposed methods' matching results in Table II. All methods run on images sized 480×640 and restrict to extracting up to 300 corners for matching. Brute force matching is used to obtain matching results for all corners with descriptors such as ORB [17]. As there is no ground truth, we match each set of frames using SIFT [16] feature points and estimate the fundamental matrix in RANSAC [29]. This matrix serves to filter all matches to obtain the correct numb. The correct match rate is the number of correct matches divided by total points.

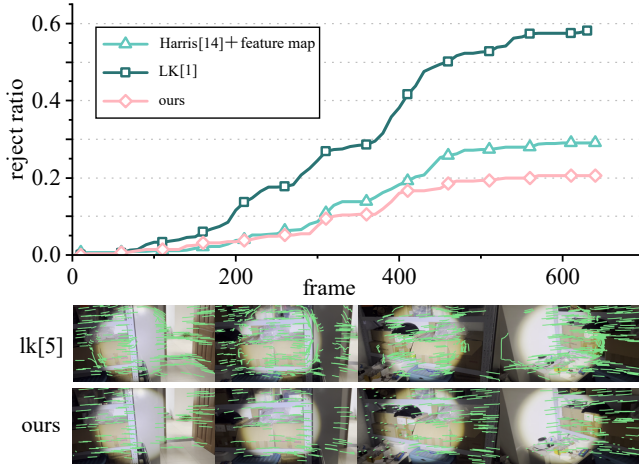


Fig. 6. **Corner tracking rejection rate.** In the sequence with active light source, the number of outliers in the optical flow matching is counted and divided by the total number of feature points to obtain the rejection rate. Compared with the original LK optical flow method, the proposed method can effectively reduce the number of outliers, thereby improving the accuracy of optical flow. And the difference between two optical flow tracking performance is shown in the form of pictures below.

Table II shows the comparison of the correct tracking rate in different scenes. From the table, we can see that the proposed method has achieved the highest correct tracking rate in all scenes. Due to the sensitivity of the traditional optical flow method to changes in illumination, it can be observed that the matching performance of the original optical flow method varies greatly between different data.

We also collected a sequence with an active light source. As in the VIO system, we continuously tracked the positions of the extracted feature points in the sequence. Fig. 6 shows that the proposed method can continuously track feature points in scenes with illumination changes. The traditional optical flow method fails due to the interference of the active light source, resulting in a rapid increase in the rejection rate.

TABLE II
CORRECT TRACKING RATIO

Scenes	Indoor	Outdoor	Image Blur	Active Lighting
Ours	0.84	0.67	0.75	0.87
Optical Flow [30]	0.58	0.45	0.19	0.37
ORB [17]	0.12	0.23	0.32	0.4
ALIKE(T) [22]	0.59	0.54	0.51	0.41
SuperPoint [19]	0.48	0.57	0.51	0.49

D. VIO Trajectory Estimation

We embed the proposed optical flow into the modern VIO system, VINS-Mono [31]. By replacing the original corner extraction algorithm and the optical flow calculation method, the modified VIO system is obtained. As shown in Fig. 7, a comparison test was performed on the UMA-VI [32] dataset with dynamic lighting data. Of these, ORB-SLAM3 [33] performed the worst, with tracking failures occurring time and time again. VINS-Mono quickly accumulates errors in

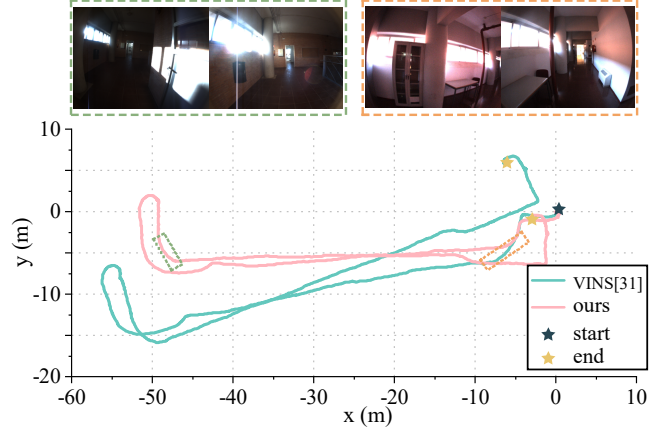


Fig. 7. **Sequence 1 trajectory graph of UMA-VI [32].** The starting point and end point of the sequence coincide, and it can be seen that the improved method can effectively improve the accuracy of the trajectory in the dynamic lighting scene. The two set of pictures corresponding to the two parts of the rapid accumulation of trajectory error are displayed above the curve, which verifies that the rapid change of lighting is the main source of error.

the trajectory in the case of changes in lighting, while the proposed method shows the highest level of accuracy. As the dataset only provides the true values of the initial and final trajectory positions, we only compute the cumulative final trajectory translation error, as shown in table III.

TABLE III
REAL TIME PERFORMANCE COMPARISON

Trajectory Error	VINS	VINS(Ours)	ORB-SLAM3
Sequence 1	8.97	2.96	lost
Sequence 2	17.81	10.67	lost

VI. CONCLUSIONS

We propose to use a shallow convolutional network to learn viewpoint and light invariant information in the image and extract corners with strong invariance. With these corner maps and feature maps, we create a new hybrid optical flow method. The proposed method no longer relies on the brightness invariance assumption of the image, which enables accurate optical flow estimation in HDR environments. To validate the proposed method, corner point repeatability is calculated on the HPatches dataset, and the results are state-of-the-art. In addition, several image sets are captured under dynamic lighting environments to verify the ability of corner tracking under dynamic lighting. Finally, the proposed optical flow is embedded in a modern VIO system and achieves higher accuracy under the public HDR dataset, which verifies its effectiveness in practical applications.

REFERENCES

- [1] B. D. Lucas and T. Kanade, “An iterative image registration technique with an application to stereo vision,” in *Int. Joint Conf. Artif. Intell.*, vol. 2, 1981, pp. 674–679.

[2] A. Dosovitskiy, P. Fischer, E. Ilg, P. Hausser, C. Hazirbas, V. Golkov, P. Van Der Smagt, D. Cremers, and T. Brox, "FlowNet: Learning Optical Flow with Convolutional Networks," in *IEEE Int. Conf. Comput. Vis. (ICCV)*, 2015, pp. 2758–2766.

[3] B. K. Horn and B. G. Schunck, "Determining optical flow," *Artif. Intell.*, vol. 17, no. 1-3, pp. 185–203, 1981.

[4] H. Zimmer, A. Bruhn, and J. Weickert, "Optic flow in harmony," *Int. J. Comput. Vis.*, vol. 93, pp. 368–388, 2011.

[5] N. Papenberg, A. Bruhn, T. Brox, S. Didas, and J. Weickert, "Highly accurate optic flow computation with theoretically justified warping," *Int. J. Comput. Vis.*, vol. 67, pp. 141–158, 2006.

[6] J.-Y. Bouguet *et al.*, "Pyramidal Implementation of the Lucas Kanade Feature Tracker Description of the algorithm," *Intel corporation*, vol. 5, no. 1-10, p. 4, 2001.

[7] T. Senst, V. Eiselein, and T. Sikora, "Robust Local Optical Flow for Feature Tracking," *IEEE Trans. Circuits Syst. Video Technol.*, vol. 22, no. 9, pp. 1377–1387, 2012.

[8] T. Senst, J. Geistert, and T. Sikora, "Robust local optical flow: Long-range motions and varying illuminations," in *IEEE Int. Conf. Image Process.*, 2016, pp. 4478–4482.

[9] H. Zhang, L. Xiao, and G. Xu, "A novel tracking method based on improved FAST corner detection and pyramid LK optical flow," in *2020 Chinese control and decision conference (CCDC)*, 2020, pp. 1871–1876.

[10] E. Ilg, N. Mayer, T. Saikia, M. Keuper, A. Dosovitskiy, and T. Brox, "FlowNet 2.0: Evolution of Optical Flow Estimation with Deep Networks," in *IEEE Conf. Comput. Vis. Pattern Recognit. (CVPR)*, 2017, pp. 2462–2470.

[11] D. Sun, X. Yang, M.-Y. Liu, and J. Kautz, "PWC-Net: CNNs for Optical Flow using Pyramid, Warping, and Cost Volume," in *IEEE Conf. Comput. Vis. Pattern Recognit. (CVPR)*, 2018, pp. 8934–8943.

[12] Z. Teed and J. Deng, "RAFT: Recurrent All-Pairs Field Transforms for Optical Flow," in *European Conference on Computer Vision*. Springer, 2020, pp. 402–419.

[13] H. Xu, J. Zhang, J. Cai, H. Rezatofighi, and D. Tao, "Gmflow: Learning optical flow via global matching," in *IEEE Conf. Comput. Vis. Pattern Recognit. (CVPR)*, 2022, pp. 8121–8130.

[14] C. Harris, M. Stephens *et al.*, "A combined corner and edge detector," in *Alvey vision conference*, vol. 15, no. 50, 1988, pp. 10–5244.

[15] J. Shi *et al.*, "Good features to track," in *IEEE Conf. Comput. Vis. Pattern Recognit. (CVPR)*. IEEE, 1994, pp. 593–600.

[16] D. G. Lowe, "Distinctive image features from scale-invariant keypoints," *Int. J. Comput. Vis.*, vol. 60, pp. 91–110, 2004.

[17] E. Rublee, V. Rabaud, K. Konolige, and G. Bradski, "ORB: An efficient alternative to SIFT or SURF," in *IEEE Int. Conf. Comput. Vis. (ICCV)*, 2011, pp. 2564–2571.

[18] X. Zhang, F. X. Yu, S. Karaman, and S.-F. Chang, "Learning discriminative and transformation covariant local feature detectors," in *IEEE Conf. Comput. Vis. Pattern Recognit. (CVPR)*, 2017, pp. 6818–6826.

[19] D. DeTone, T. Malisiewicz, and A. Rabinovich, "Superpoint: Self-supervised interest point detection and description," in *IEEE Conf. Comput. Vis. Pattern Recognit. (CVPR)*, 2018, pp. 224–236.

[20] M. Dusmanu, I. Rocco, T. Pajdla, M. Pollefeys, J. Sivic, A. Torii, and T. Sattler, "D2-net: A trainable cnn for joint description and detection of local features," in *IEEE Conf. Comput. Vis. Pattern Recognit. (CVPR)*, 2019, pp. 8092–8101.

[21] A. Barroso-Laguna, E. Riba, D. Ponsa, and K. Mikolajczyk, "Key. net: Keypoint detection by handcrafted and learned cnn filters," in *IEEE Int. Conf. Comput. Vis. (ICCV)*, 2019, pp. 5836–5844.

[22] X. Zhao, X. Wu, J. Miao, W. Chen, P. C. Chen, and Z. Li, "Alike: Accurate and lightweight keypoint detection and descriptor extraction," *IEEE Trans. Multimed.*, 2022.

[23] X. Glorot, A. Bordes, and Y. Bengio, "Deep sparse rectifier neural networks," in *Proceedings of the fourteenth international conference on artificial intelligence and statistics*, 2011, pp. 315–323.

[24] H. Germain, V. Lepetit, and G. Bourmaud, "Neural Reprojection Error: Merging Feature Learning and Camera Pose Estimation," in *IEEE Conf. Comput. Vis. Pattern Recognit. (CVPR)*, 2021, pp. 414–423.

[25] V. Balntas, K. Lenc, A. Vedaldi, and K. Mikolajczyk, "HPatches: A benchmark and evaluation of handcrafted and learned local descriptors," in *IEEE Conf. Comput. Vis. Pattern Recognit. (CVPR)*, 2017, pp. 5173–5182.

[26] Z. Li and N. Snavely, "MegaDepth: Learning Single-View Depth Prediction From Internet Photos," in *IEEE Conf. Comput. Vis. Pattern Recognit. (CVPR)*, June 2018.

[27] D. P. Kingma and J. Ba, "ADAM: A method for stochastic optimization," *preprint arXiv:1412.6980*, 2014.

[28] M. Trajković and M. Hedley, "Fast corner detection," *Image and vision computing*, vol. 16, no. 2, pp. 75–87, 1998.

[29] M. A. Fischler and R. C. Bolles, "Random sample consensus: a paradigm for model fitting with applications to image analysis and automated cartography," *Communications of the ACM*, vol. 24, no. 6, pp. 381–395, 1981.

[30] J.-Y. Bouguet *et al.*, "Pyramidal Implementation of the affine Lucas Kanade Feature Tracker Description of the Algorithm," *Intel corporation*, vol. 5, no. 1-10, p. 4, 2001.

[31] T. Qin, P. Li, and S. Shen, "VINS-Mono: A robust and versatile monocular visual-inertial state estimator," *IEEE Trans. Robotics*, vol. 34, no. 4, pp. 1004–1020, 2018.

[32] D. Zuñiga-Noël, A. Jaenal, R. Gomez-Ojeda, and J. Gonzalez-Jimenez, "The UMA-VI dataset: Visual-inertial odometry in low-textured and dynamic illumination environments," *Int. J. Rob. Res.*, vol. 39, no. 9, pp. 1052–1060, 2020.

[33] C. Campos, R. Elvira, J. J. G. Rodríguez, J. M. Montiel, and J. D. Tardós, "ORB-SLAM3: An accurate open-source library for visual, visual-inertial, and multimap slam," *IEEE Trans. Robotics*, vol. 37, no. 6, pp. 1874–1890, 2021.